HiSST: 2nd International Conference on
High-Speed Vehicle Science Technology
11–15 September 2022, Bruges, Belgium

Reaction Mechanism Reduction for Ethylene-Fueled Supersonic Combustion CFD

Kan Kobayashi[1], Sadatake Tomioka[2], Masahiro Takahashi[3], and Masatoshi Kodera[4]

Abstract

To build a reduced reaction mechanism for 3D simulation of C2H4/Air reaction in supersonic combustion ramjet combustor, CHEMKIN-Pro was used. USC Mech II (111 species mechanism) was applied as a master mechanism. First, 1D simulation was conducted by applying so-called plug flow reactor model and 34, 23, 20, 18, and 19 species mechanisms were suggested as candidates of reduced mechanisms. In addition, 0D ignition delay simulation by applying so-called perfectly stirred reactor model by CHEMKIN-Pro, 2D reacting flow simulation by CRUNCH CFD, and 3D reacting flow simulation by RANS were performed to choose the most suitable reduced model. As a result, the 20 species (96 reactions) mechanism which consists of H2, O2, N2, H2O, CO2, CO, H, O, OH, HO2, CH2, CH2*, CH3, HCO, CH2O, CH3O, C2H2, C2H3, C2H4, and CH2CHO was selected as the best reduced reaction mechanism for C2H4 fueled 3D simulation.

Keywords: *Propulsion, Scramjet Engine, Flight Test, Combustion Simulation, Reaction Mechanism*

1. Introduction

In relation to the flight test of the scramjet combustor conducted by JAXA, a reaction mechanism applicable to 3D reacting flow simulation is required to understand the phenomena in the combustor. Since the flight model is an air-breathing engine using C2H4 (ethylene) as fuel, a C2H4/Air reaction mechanism is required. Although some reduced reaction mechanisms applicable to C2H4/Air reaction simulations have been proposed, the reproducibility of reactions changes depending on the phenomena focused on. Therefore, it is difficult to find a versatile reaction mechanism from existing reduced mechanisms. Using the commercially available code CHEMKIN-Pro [1], some reductions of the detailed C2H4/Air reaction mechanism (more than 100 chemical species) are attempted for the flight model combustor in this study. The target number of chemical species is around 20 after reduction. Note that the goal of the present study is to establish a method to build a custom-made reaction mechanism for a specific target, rather than aiming at constructing a versatile reaction mechanism applicable to many targets due to the background described above.

2. Simplification of target flow field to 1D simulation

In the reduction of the reaction mechanism in CHEMKIN-Pro, the user specifies the simulation target and simulation conditions of interest, while referring to the results obtained from the detailed reaction mechanism (which is also specified by the user). The number of chemical species is gradually reduced while monitoring to minimize deviations from the results with a detailed reaction mechanism, namely, a master reaction mechanism. In other words, the simulation target applied to this work must be a simulation to which the detailed reaction mechanism can be applied. Therefore, even if the goal is a 3D reacting flow simulation, it must first be replaced with a lower dimensional simulation. The simulation target of this report is the 3D flow field with reaction in the flight model combustor. Thus, this 3D flow field in the combustor is replaced with a 1D flow field in this section.

[1] *Japan Aerospace Exploration Agency (JAXA), Kakuda, Miyagi 981-1525, JAPAN, kobayashi.kan@jaxa.jp*
[2] *Japan Aerospace Exploration Agency (JAXA), Kakuda, Miyagi 981-1525, JAPAN, tomioka.sadatake@jaxa.jp*
[3] *Japan Aerospace Exploration Agency (JAXA), Kakuda, Miyagi 981-1525, JAPAN, masahiro.takahashi@jaxa.jp*
[4] *Japan Aerospace Exploration Agency (JAXA), Kakuda, Miyagi 981-1525, JAPAN, kodera.masatoshi@jaxa.jp*

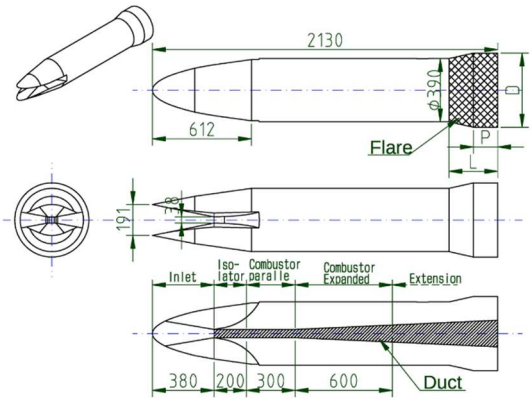

Fig. 1 Conceptual structure of flight model

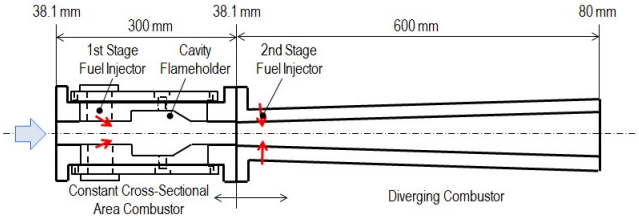

Fig. 2 Combustor section

Figure 1 shows a conceptual structure of the flight model. The airflow enters from the opening in the front, is compressed by a ramp compression unit (inlet) with a length of 380 mm, and passes through a constant cross-sectional area duct (isolator) with a length of 200 mm. It flows into the 300 mm constant cross-sectional area combustor. After that, it flows out of the exhaust duct through the diverging combustor having a length of 600 mm. Figure 2 shows the structural outline of the combustor section with a length of 300 mm + 600 mm. The cavity flame holder in the constant cross-sectional area combustor ensures enough residence time longer than the reaction time by circulating a part of the flow of high-speed air and fuel to ensure ignition and flame holding.

The purpose of this study is related to the fact that fuel injection is divided into the first and second stages. In the facility test under high airflow total temperature, the airflow includes H2O because when the total temperature is too high to be achieved by the storage heating method, the heating method using lean combustion of H2 is adopted. One of the purposes of this study is to investigate the influence of this H2O in the facility test on combustion characteristics. That is, it is necessary to detect a difference in combustion reaction under two different airflow conditions, namely, facility condition (with H2O) and flight condition (without H2O). For this purpose, it is desirable to burn in an environment where the progress of the combustion reaction is moderately slow, that is, in an appropriate low temperature and pressure environment. Therefore, it is required to inject fuel in the diverging combustor in which the flow path expands, and the static temperature and pressure gradually decrease. On the other hand, the airflow at the diverging combustor inlet is not so high in static temperature and pressure that C2H4 combustion can be achieved. Therefore, it is required that a part of the fuel is burned in the constant cross-sectional area combustor, and the static temperature and pressure of the airflow at the diverging combustor inlet are increased to some extent. Based on the above, it was decided to adopt a two-stage fuel injection system, the first stage injection from the constant cross-sectional area combustor and the second stage injection from the diverging combustor. Note that it was found that the optimal equivalence ratio is 0.25 in each stage (total equivalence ratio is 0.5) and the optimal diverging angle of the diverging combustor is 2 degrees on each side (total diverging angle is 4 degrees) in this combustor.

The purpose of the 3D reacting flow simulation is to reproduce the difference in combustion, especially in the diverging combustor, under two airflow conditions (flight and facility conditions). Therefore, the simulation applied to the reaction mechanism reduction needs to approximate the flow field in the diverging combustor in 1D. In this report, it is considered that C2H4 with an equivalence ratio of 0.25 injected from the first stage and air are premixed and the equilibrium combustion gas that has reached the equilibrium state (O2 remains because of the lean combustion) flows into the diverging combustor. After the combustion gas flows into the diverging combustor, the flow field changes (static temperature and pressure decrease) according to the expansion of the flow path up to the second stage fuel injection location. At the second stage fuel injection location, C2H4 with an equivalence ratio of 0.25 and the equilibrium combustion gas at that location mix instantly and the reaction starts from that location. From the above, in the reduction of the reaction mechanism that also needs to apply the detailed reaction mechanism, the cross section is homogeneous at each location in the flow direction, and the so-called "plug flow" in which the state in the cross section including the cross-sectional area changes in the flow direction was adopted. After applying the plug flow reactor model, a 1D reacting flow simulation is performed within the area from the second stage fuel injection location to the diverging combustor exit.

3. Reaction mechanism reduction by CHEMKIN-Pro with 1D simulation

3.1 1D simulation by "plug flow reactor" model

In flight and facility conditions, the most suitable measurement target for detecting the difference in combustion in the diverging combustor is the static pressure distribution in terms of ease of measurement. The static pressure distribution is also used for evaluation of thrust performance, which is particularly important in engine performance. Therefore, this study emphasizes the static pressure distribution. Also, in the reduction of the reaction mechanism, which will be described later, the static pressure distribution is particularly focused on from the simulation results obtained by the detailed reaction mechanism, and the reduction is advanced so that this can be accurately reproduced. In this section, prior to reduction of the reaction mechanism, a detailed reaction mechanism is used, and then a 1D reacting flow simulation using a plug flow reactor model is performed. The optimum condition (i.e., the location where the difference in static pressure distribution between flight and facility conditions is most easily detected) is explored. The simulation conditions were fixed at the first stage equivalence ratio of 0.25, the second stage equivalence ratio of 0.25 (0.5 in total) and a diverging angle of 2 degrees on each side (4 degrees in total). The second stage fuel injection location, where the 1D reacting flow simulation starts, is changed as 0, 0.09, 0.18, and 0.27 m from the diverging combustor entrance, and the various distributions under flight and facility conditions are examined. As a detailed reaction mechanism, USC Mech II [2] (111 chemical species 770 elementary reactions) that can reproduce the ignition delay obtained in the shock tube test [3] was adopted.

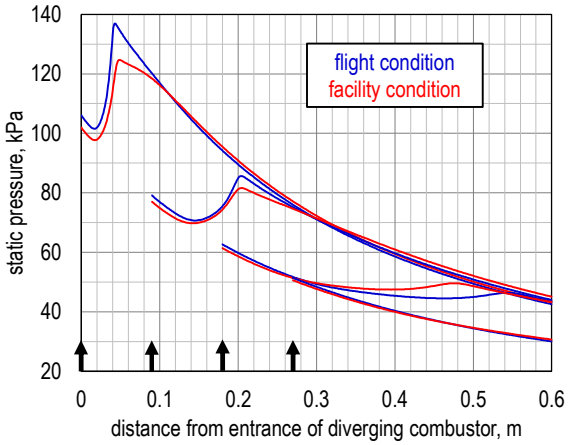

Fig. 3 Static pressure distributions

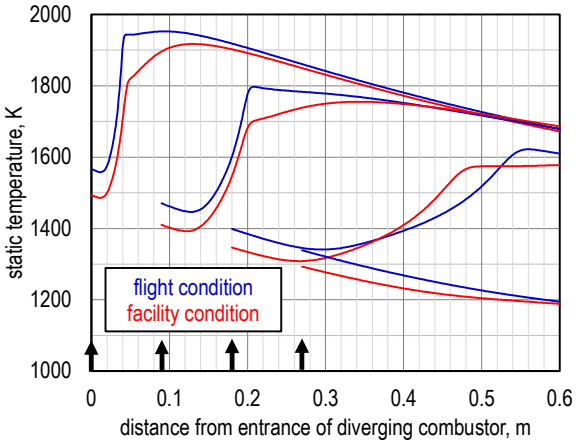

Fig. 4 Static temperature distributions

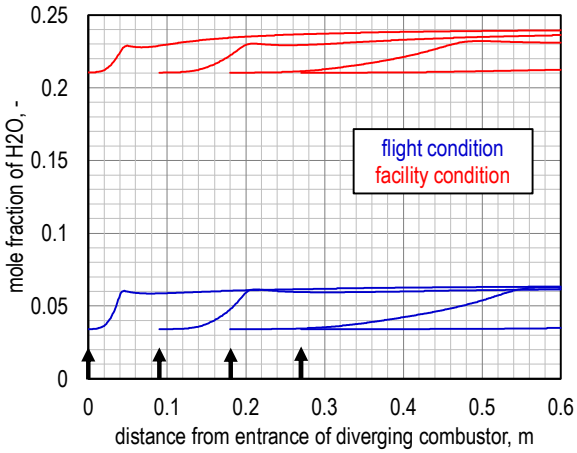

Fig. 5 H2O mole fraction distributions

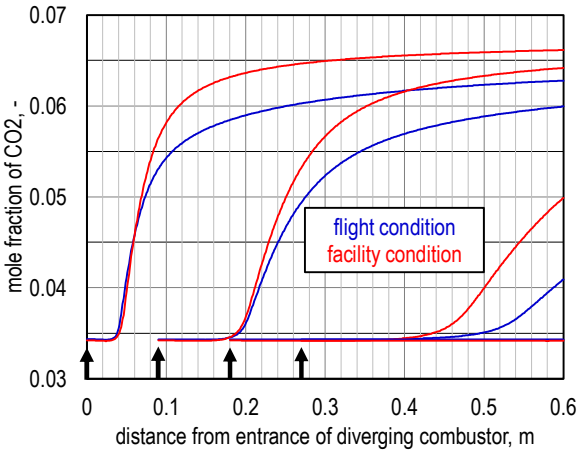

Fig. 6 CO2 mole fraction distributions

Figure 3 shows the static pressure distributions. When the second stage fuel injection location is 0 and 0.09 m, the peak pressure location is almost the same between flight and facility conditions. At these locations, the static temperature and pressure are relatively high, and the reaction is too fast to detect the difference. When the second stage fuel injection location is 0.18 m, there is an increase in static pressure due to combustion, and there is a difference in the peak location between flight and

facility conditions. When the second stage fuel injection location is 0.27 m, no static pressure increase due to heat release was observed under any conditions. At this location, the static temperature and pressure are relatively low, and the reaction is too slow to detect the difference. Based on the above, this report uses the static pressure distribution at the second stage fuel injection location of 0.18 m, where the difference between flight and facility conditions was most noticeable, to reduce and verify the reaction mechanism. Figure 4 shows the static temperature distributions. At the second stage fuel injection locations of 0 and 0.09 m, the static temperature rise is almost the same, but the subsequent increase in static temperature is somewhat slower under the facility condition. Here, the effect of static temperature decreases by expanding the flow path and the effect of static temperature rise by heat release compete. Under the facility condition that contains H2O in the air stream, exothermic reactions are suppressed by the existing H2O. At the second stage fuel injection location of 0.18 m, the static temperature rises faster in the facility condition, but heat release continues to compete the effect of channel expansion downstream from the static pressure peak location. Under the flight condition, the static temperature rises slowly, but the static temperature decreases downstream from the peak location. The static temperature rise is slow until the start of the reaction but fast until the completion of the subsequent reaction. The static temperature distribution also shows that the second stage fuel injection location of 0.18 m is suitable when detecting the difference in the results between flight and facility conditions as the difference in peak location. By comparing with the H2O distribution (Fig. 5) and CO2 distribution (Fig. 6) obtained in this simulation, it was found that the static temperature and pressure increase process corresponds to the H2O production process and the subsequent process after the peak corresponds to the CO2 production process. In other words, the first half of C2H4 combustion consists mainly of H2 combustion and the second half mainly consists of CO combustion.

3.2 Reduction of C2H4/Air reaction mechanism by "reaction workbench"

The reduction of the detailed reaction mechanism was performed by using CHEMKIN-Pro in this section. USC Mech II was designated as the detailed reaction mechanism (master mechanism). In addition, the static pressure distribution under the facility condition at the second stage fuel injection location of 0.18 m selected in the previous section was specified as an index used for reproducibility judgment during the reduction process. Furthermore, it is assumed that, for example, 10% is given as an allowable error for the static pressure distribution. Then, CHEMKIN-Pro automatically proceeds with the following operations.

(A) Calculate the static pressure distribution with USC Mech II (master mechanism).
(B) Delete low impact species and related reactions.
(C) Calculate the static pressure distribution using the reduced reaction mechanism created in (B).
(D) Calculate the error in (C) from the comparison between (A) and (C).
(E) If the result of (D) is 10% or less, perform (B)-(D) again and otherwise reduction is stopped.

Note that there are some methods in (B) as shown later. The user specifies one of them in advance.

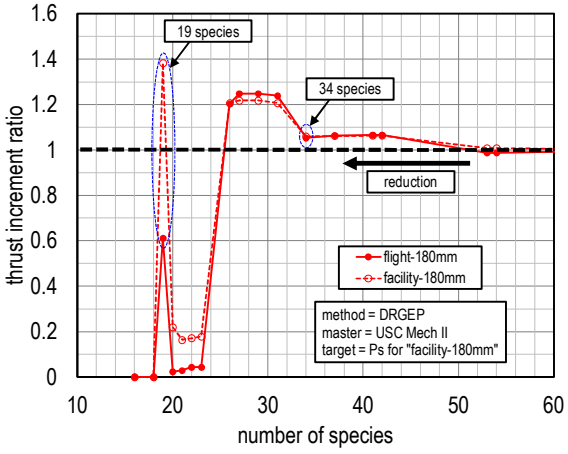

Fig. 7 Reduction by DRGEP method

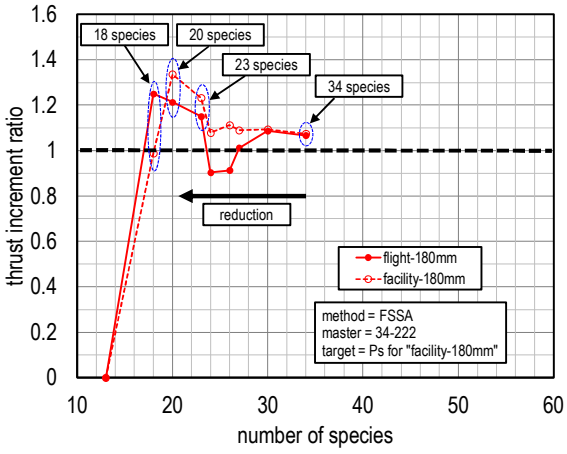

Fig. 8 Reduction by FSSA method

Figure 7 shows the relationship between the integral pressure thrust increment ratio and the number of species. The integral pressure thrust (F_p) is obtained from the static pressure distribution. The integral pressure thrust increment (ΔF_p) is defined as the difference between F_p with reaction and F_p without reaction, shown as Eq. 1.

$$\Delta F_p = F_p\big|_{reac.} - F_p\big|_{no-reac.} \tag{1}$$

The integral pressure thrust increment ratio (r) is defined as the ratio of ΔF_p with reduced reaction mechanism and ΔF_p with detailed reaction mechanism, shown as Eq. 2.

$$r = \frac{\Delta F_p|_{reduced}}{\Delta F_p|_{detailed}} = \frac{\left(F_p|_{reac.} - F_p|_{no-reac.}\right)_{reduced}}{\left(F_p|_{reac.} - F_p|_{no-reac.}\right)_{detailed}} \tag{2}$$

Therefore, when the static pressure distribution by the reduced reaction mechanism matches that calculated by the detailed reaction mechanism, r equals to unity, and the larger the deviation from unity, it shows the worse the reproducibility of the static pressure distribution. Here, DRGEP (Directed Relation Graph with Error Propagation) method [4, 5] was used as the reduction method of (B) above. To observe how the reproducibility of the static pressure distribution deteriorates due to reduction, a large value (larger than 10%) was given as an allowable error here.

Reduction of the reaction mechanism proceeds from right to left in the figure. As the number of species is reduced, the reproducibility deteriorates step by step. For example, in Fig. 7, after maintaining a relatively good reproducibility up to 34 species, if the number of species falls below 34, a large shift occurs, and a significant deviation occurs at 23 species or less. Note that when the number of species falls below 18, the integral pressure thrust increment ratio (r) becomes zero. This is a case in which fuel and air flow out of the diverging combustor before the occurrence of reaction although the reaction occurs in the diverging combustor when using the detailed reaction mechanism. One interesting feature of Fig. 7 is that 19 species mechanism specifically reduce the deviation compared to 20-23 species mechanisms and improve the reproducibility. This 19 species mechanism was included as a candidate of reduced mechanism.

In CHEMKIN-Pro, FSSA (Full Species Sensitivity Analysis) method is also suggested as the final step of reduction after some reductions are done by DRGEP method. Here, 34 species mechanism was selected as the master mechanism for FSSA method because this is the smallest mechanism in which the deviation in the integral pressure thrust increment (r) is within 10% in the DRGEP method. Figure 8 shows the relationship between the number of species and r, obtained by FSSA method. To observe how the reproducibility of the static pressure distribution deteriorates due to reduction, a large value (larger than 10%) was given as an allowable error here. 34, 23, 20, and 18 species mechanisms were focused on as candidates of reduced mechanism. Note that the reaction does not occur in the diverging combustor when the number of species is 13 or less.

As a result, 34, 23, 20, and 18 species mechanisms were selected as the primary candidates and 19 species mechanism was selected as the secondary one. These candidates are compared to 111 species mechanism (USC Mech II) in this report. Table 1 shows that the deviation in the integral pressure thrust increment ratio (r) of these five reduced mechanisms was around 40% at most in the case of the 19 species mechanism under flight and facility conditions. In the table, the captions show the set of the numbers of species and reactions. For example, 111-770 means 111 species and 770 reactions. The set of species for these reduced mechanisms are shown in Table 2. As can be seen in the table, 19-71 is categorised into a different group from other reduced mechanisms.

Table 1 Integral pressure thrust increment ratio (r) for reduced mechanisms

	111-770	34-222	23-121	20-96	18-63	19-71
flight	1 (ref.)	1.066	1.151	1.213	1.250	0.611
facility	1 (ref.)	1.074	1.232	1.336	0.987	1.382

For the 34, 23, 20, 18, and 19 species mechanisms, the comparison results with the detailed reaction mechanism (111 species) focusing on the static pressure distribution for 0.18 m injection are shown in Fig. 9 (flight condition) and Fig. 10 (facility condition). The static temperature distributions are also shown in Fig. 11 (flight condition) and Fig. 12 (facility condition). Comparing to the result for 111 species, the results for 34 and 23 species show a good reproducibility. Among these three mechanisms (111-770, 34-222, and 23-121), the common feature that the reductions result in the

reaction promotion can be seen for both static pressure and temperature. The result for 20 species shows a similar profile to that for 23 species, but the profile becomes sluggish. The result for 18 species shows a different trend from the mechanisms mentioned above. Comparing to the result for 111 species, the heat release is faster as seen in Figs. 9-12. The peak pressure is higher for both conditions (Figs. 9 and 10), but the peak temperature is lower for both conditions (Figs. 11 and 12). The result for 19 species shows different (or opposite) feature between flight and facility conditions. Comparing to the result for 111 species, the heat release is slower under flight condition (Figs. 9 and 11), but it is faster under facility condition (Figs. 10 and 12). From 1D analysis, it seems that 34-222 and 23-121 are "excellent," 20-96 is "fair," and 18-63 and 19-71 is "poor" regarding the reproducibility of the result of 111-770.

Table 2 Species included in reduced mechanisms

No.	species	34-222	23-121	20-96	18-63	19-71
1	N2	●	●	●	●	●
2	H	●	●	●	●	●
3	O	●	●	●	●	●
4	OH	●	●	●	●	●
5	HO2	●	●	●	●	●
6	H2	●	●	●	●	●
7	H2O	●	●	●	●	●
8	O2	●	●	●	●	●
9	CH2*	●	●	●	●	●
10	CH3	●	●	●	●	●
11	HCO	●	●	●	●	●
12	CO	●	●	●	●	●
13	CO2	●	●	●	●	●
14	C2H3	●	●	●	●	●
15	C2H4	●	●	●	●	●
16	CH2CHO	●	●	●	●	●
17	CH3O	●	●	●	●	-
18	C2H2	●	●	●	●	-
19	CH2	●	●	●	-	●
20	CH2O	●	●	●	-	-
21	CH4	●	●	-	-	-
22	CH3OH	●	●	-	-	-
23	HCCO	●	●	-	-	-
24	H2CC	●	-	-	-	●
25	C2H5	●	-	-	-	●
26	CH2OH	●	-	-	-	-
27	C2O	●	-	-	-	-
28	H2O2	●	-	-	-	-
29	CH	●	-	-	-	-
30	C2H6	●	-	-	-	-
31	CH2CO	●	-	-	-	-
32	pC3H4	●	-	-	-	-
33	aC3H4	●	-	-	-	-
34	aC3H5	●	-	-	-	-

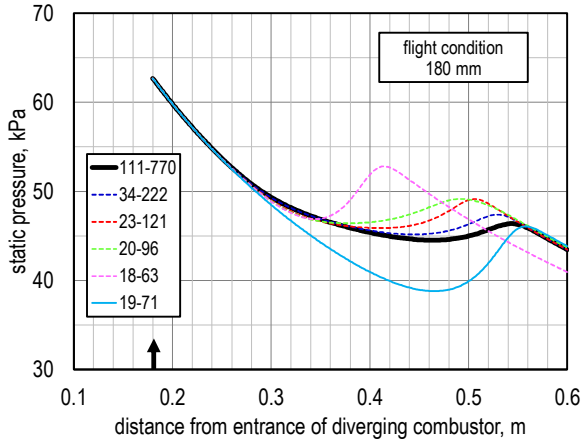

Fig. 9 Master vs. reduced (flight condition) Static pressure profile

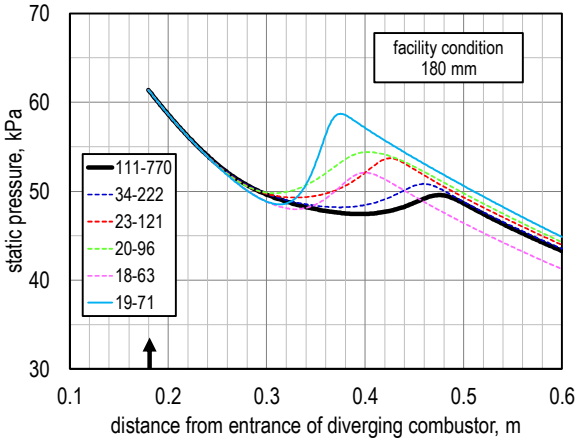

Fig. 10 Master vs. reduced (facility condition) Static pressure profile

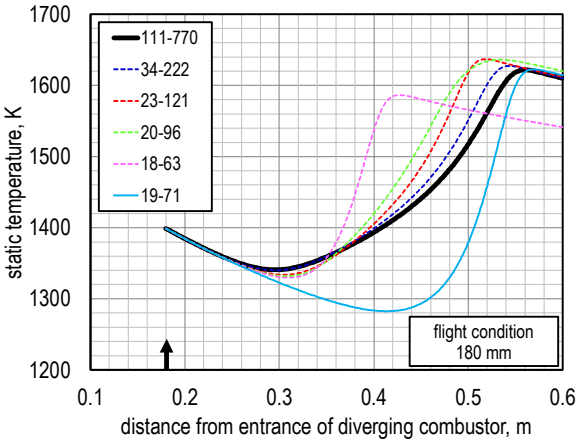

Fig. 11 Master vs. reduced (flight condition) Static temperature profile

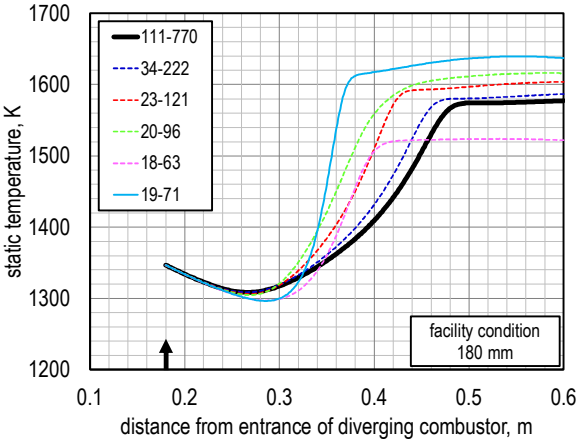

Fig. 12 Master vs. reduced (facility condition) Static temperature profile

4. <u>Validation 1</u>: 0D ignition delay simulation by "perfectly stirred reactor" model

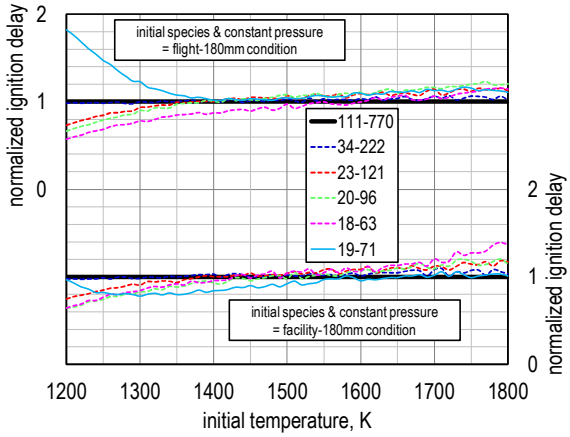

Fig. 13 Normalized ignition delay

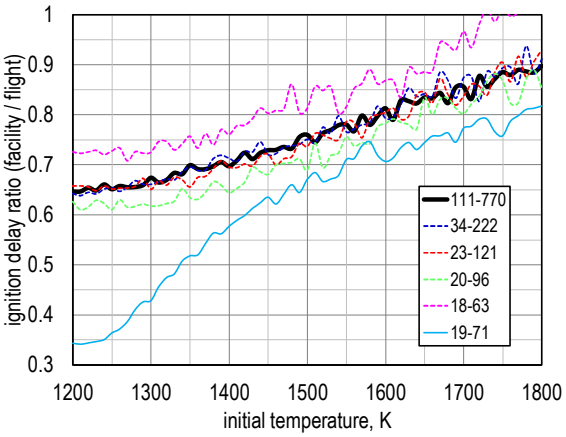

Fig. 14 Ignition delay ratio

In this section, the ignition delay was evaluated in a perfectly stirred reactor (PSR) model that can be simulated with CHEMKIN-Pro as another index for selecting a reduced reaction mechanism. The simulation conditions are based on facility and flight conditions at 0.18 m injection, and the initial composition at 0.18 m injection is given, and the initial temperature is 1200-1800 K to include the initial static temperature at 0.18 m injection. The initial static pressure for 0.18 m injection was used as a

constant pressure. Ignition is defined as the moment at which dT/dt is maximum, and the required time from the start of calculation to ignition is defined as the ignition delay.

Figure 13 shows the relationship between initial temperature and ignition delay. As candidates for the reduced reaction mechanism, all sets of 34, 23, 20, 18, and 19 species that appeared in the previous section were examined. The upper half shown with the left axis is the results under flight condition, and the lower half shown with the right axis is the results under facility condition. The ignition delay was normalized by that calculated with the detailed reaction mechanism (111-770) which is a reproduction target. Therefore, the closer the vertical axis value is to unity, the better the reproducibility of the ignition delay in the detailed reaction mechanism. It is interesting that the reductions result in ignition promotion below 1500 K and result in ignition suppression above 1500 K except for 19 species mechanism. Ignition delay for 34 and 23 species mechanisms shows a better reproducibility comparing to that for 20, 18, and 19 species mechanisms.

Figure 14 shows the ratio of the ignition delay under facility condition to that under flight condition. The purpose of this study is to reproduce the difference between these two conditions. Therefore, when focusing on the ignition delay, the ratio between these two conditions is important in addition to the ignition delay itself. The common feature of all reaction mechanisms is that the ignition delay under facility condition is shorter than that under flight condition. This corresponds to the fact that the static pressure peak appears more upstream in the facility condition in Figs. 9 and 10 (except for 18-63), and the result of the 1D simulation that calculated the static pressure distribution and the 0D simulation that calculated the ignition delay are consistent. As a reduced reaction mechanism, if you select one that reproduces the ignition delay ratio of the detailed reaction mechanism well, the 34 or 23 species mechanism is a candidate, and the same conclusion as in the previous 1D simulation was obtained. It seems that 34-222 and 23-121 are "excellent," 20-96 is "fair," and 18-63 and 19-71 is "poor" regarding the reproducibility of the result of 111-770.

5. Validation 2: 2D reacting flow simulation

In this section, using the reduced mechanism candidates obtained so far, 2D reacting flow simulation was conducted by using the commercially available code CRUNCH CFD [6]. The 2D simulation is closer to the actual combustion field than 0D and 1D simulations because it can include diffusion and mixing processes. Since it is possible to apply a detailed reaction mechanism with a 2D reacting flow simulation, the effectiveness of each candidate can be directly verified. As the reaction mechanisms adopted in this section, in addition to the detailed reaction mechanism (111 species), 34, 23, 20, 18, and 19 species were selected. The target of simulation was the diverging combustor, like the 1D reacting flow simulation. C2H4/Air equilibrium combustion gas corresponding to the first stage fuel (equivalence ratio of 0.25) flows into the diverging combustor inlet, diffusion and mixing with the second stage fuel (equivalence ratio of 0.25) is occurred, and then, the combustion reaction starts. Regarding the second stage fuel injection location, 0.18 m was the best in the 1D reacting flow simulation, but the situation could change in the 2D reacting flow simulation. Therefore, it was set at 0 m to have the longest residence time in the combustor. In the actual combustor, the second stage fuel is injected perpendicularly to the wall surface from the circular hole injectors, whereas in this simulation, it is injected parallel to the mainstream from the wall side slit. This is because the objective of this simulation is not to reproduce the actual flow field but to compare the feature of reaction between the detailed reaction mechanism and the reduced reaction mechanism with a simple flow field as much as possible. To suppress the generation of waves as much as possible, parallel fuel injection was applied after equalizing the static pressure of the fuel injection section with the static pressure of the main flow.

Figures 15 and 16 show the static pressure [Pa] and static temperature [K] distributions under flight and facility conditions, respectively. Since the main flow is a parallel flow at the entrance of diverging combustor (= the exit of constant cross-sectional area combustor), an expansion wave from the entrance of diverging combustor is inevitable in the static pressure profiles. The wave structure visible in the figure starts with this expansion wave. Since the equilibrium combustion gas from the constant cross-sectional area combustor flows into the diverging combustor section, the temperature of the entire analysis field is relatively high (static temperature of about 1600 K). The second stage fuel is injected parallel to the mainstream at the entrance of the diverging combustor, that is, at an angle of 2 degrees with respect to the wall of the diverging combustor. The reaction region gradually develops in the vicinity of the wall surface in the static temperature profiles. Looking at the profiles in Figs. 15 and 16, there is almost no difference in the results of 34, 23, 20, and 18 species compared to the result of 111 species. Only 19 species mechanism shows a different result from those by other mechanisms.

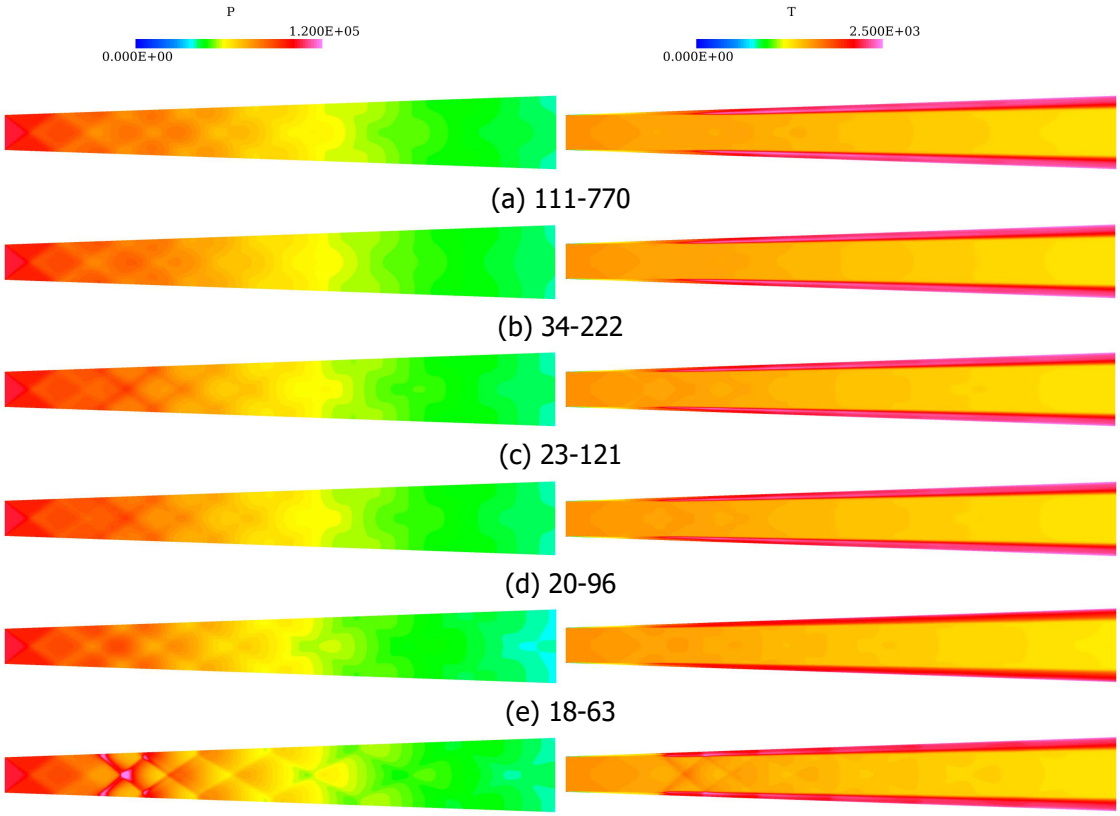

(a) 111-770

(b) 34-222

(c) 23-121

(d) 20-96

(e) 18-63

(f) 19-71

Fig. 15 2D contour of static pressure (left) and static temperature (right) for flight condition

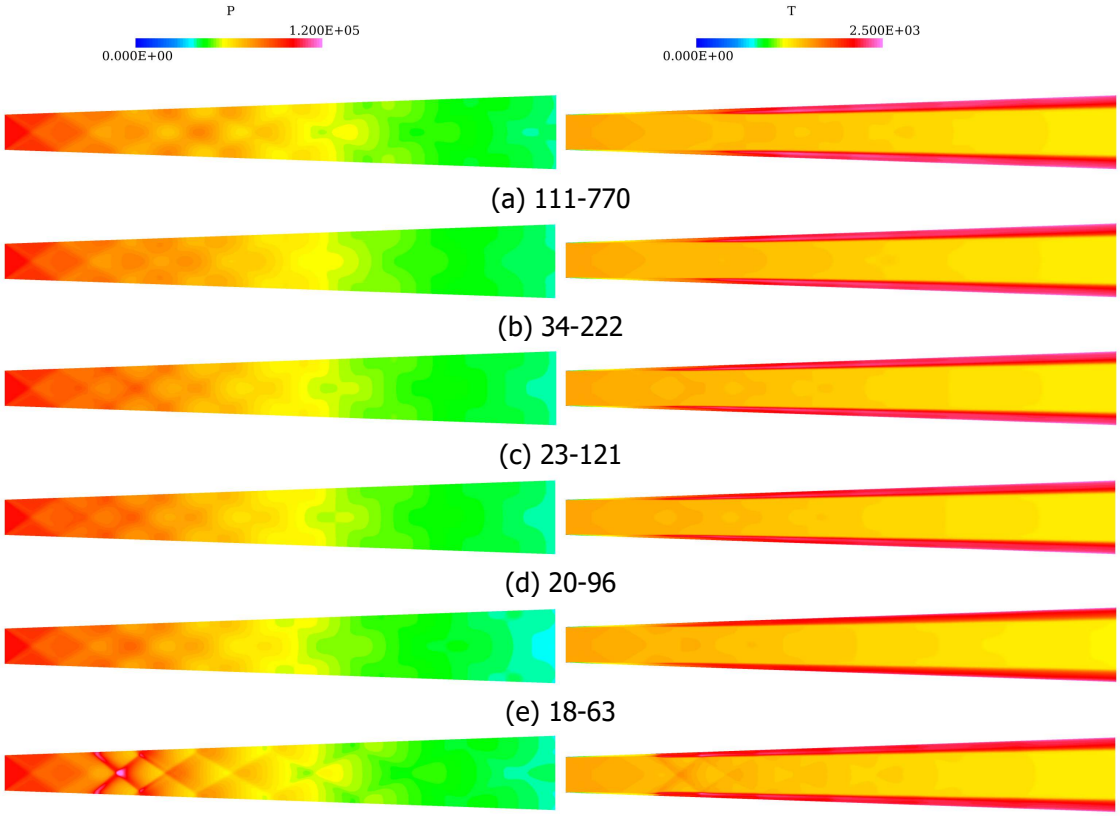

(a) 111-770

(b) 34-222

(c) 23-121

(d) 20-96

(e) 18-63

(f) 19-71

Fig. 16 2D contour of static pressure (left) and static temperature (right) for facility condition

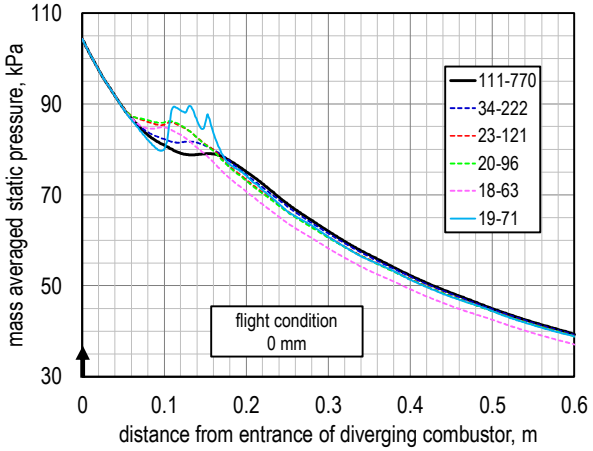

Fig. 17 Master vs. reduced (flight condition) Mass averaged static pressure profile

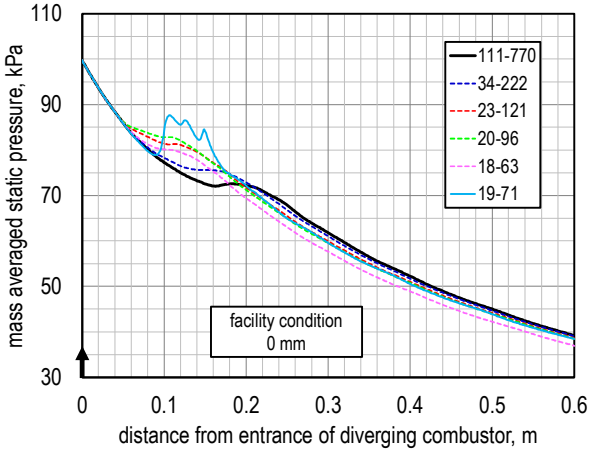

Fig. 18 Master vs. reduced (facility condition) Mass averaged static pressure profile

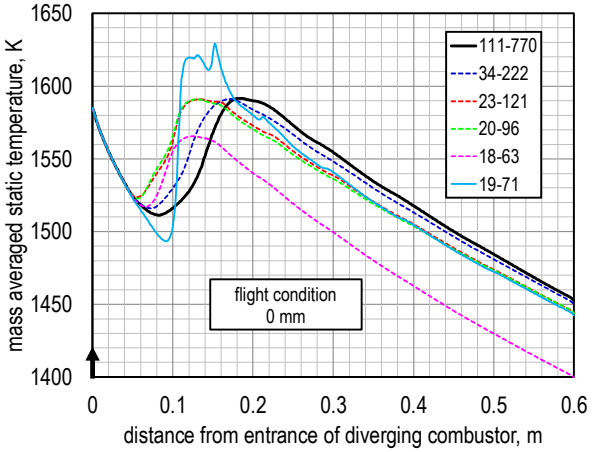

Fig. 19 Master vs. reduced (flight condition) Mass averaged static temperature profile

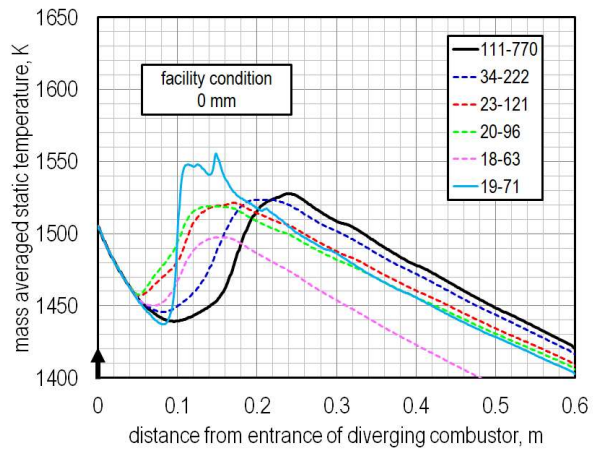

Fig. 20 Master vs. reduced (facility condition) Mass averaged static temperature profile

The static pressure distribution in X direction on the wall surface is undulating due to the incidence of waves, making it difficult to compare the results among these reaction mechanisms. Therefore, the distributions of the mass flow weighted average values of static pressure for these six reaction mechanisms (111, 34, 23, 20, 18, and 19 species mechanisms) are shown in Fig. 17 (flight condition) and Fig. 18 (facility condition). The features in Figs. 17 and 18 are the same. As the reduction progresses, the reaction is accelerated, and the static pressure peak location shifts to the upstream side. Further, although the difference is slight, when Fig. 17 is compared with Fig. 18, the degree of reaction promotion is greater in Fig. 18 (facility condition). The above features about static pressure are consistent with the results of the 1D reacting flow simulation shown in Figs. 9 and 10. In addition, the distributions of the mass flow weighted average values of static temperature are shown in Fig. 19 (flight condition) and Fig. 20 (facility condition). The same features that the reaction is accelerated, and the static temperature peak location shifts to the upstream side as the reduction progresses and the degree of reaction promotion is greater in Fig. 20 (facility condition) are shown. Note that static temperature profile for 18 species mechanism shows different trend from other four mechanisms (111-770, 34-222, 23-121, and 20-96), namely, lower static temperature. The above features about static temperature are consistent with the results of the 1D reacting flow simulation shown in Figs. 11 and 12. In addition, 19 species mechanism shows clearly different static pressure and temperature profiles from other five mechanisms (111-770, 34-222, 23-121, 20-96, and 18-63). The profiles of 19 species mechanism have multiple peaks, indicating that these peaks are not due to reaction, but due to local wave interference as can be seen in Figs. 15(f) and 16(f). From 2D analysis, it seems that 34-222 is "excellent," 23-121 and 20-96 are "fair," and 18-63 and 19-71 is "poor" regarding the reproducibility of the result of 111-770.

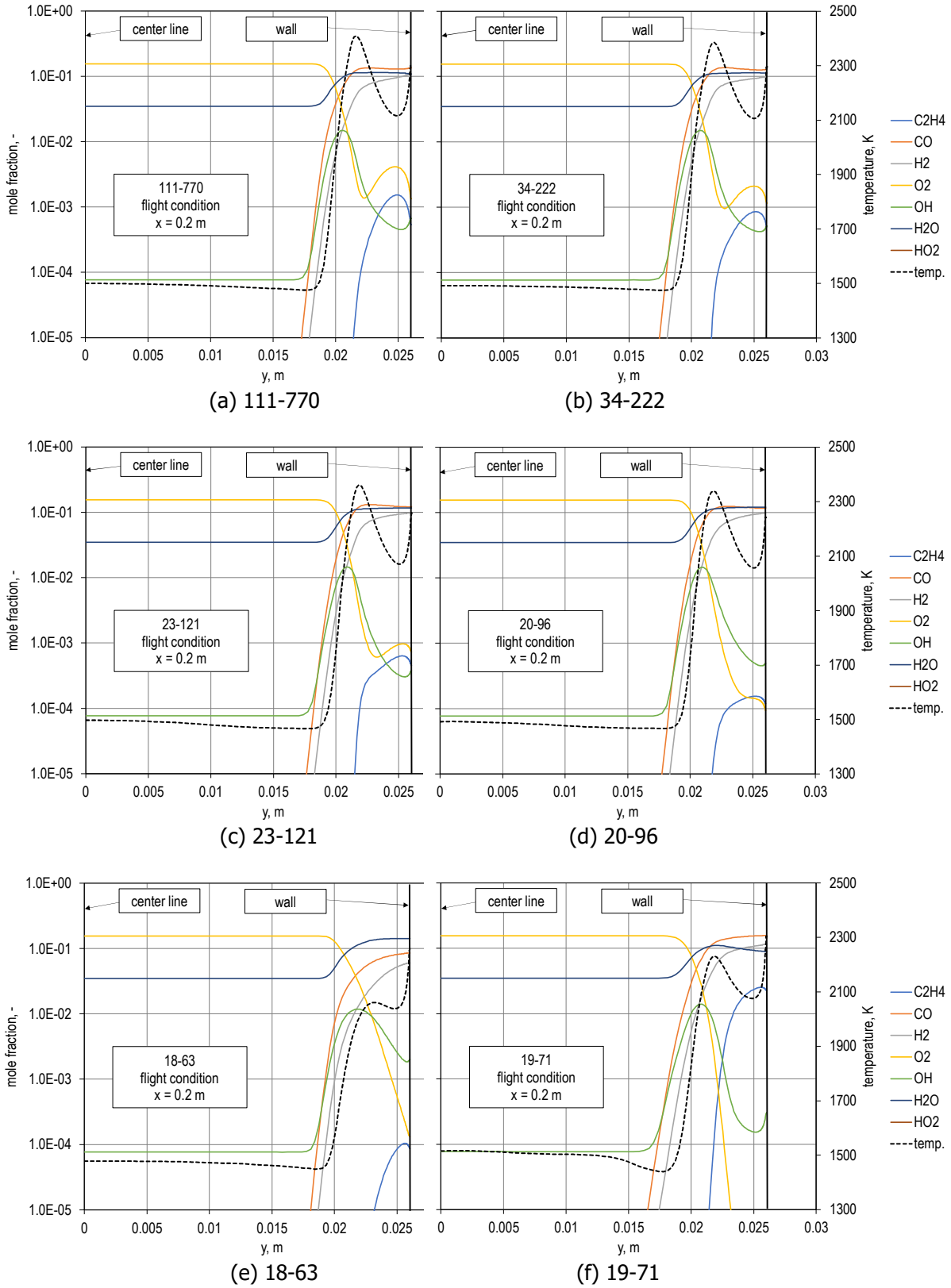

(a) 111-770 (b) 34-222

(c) 23-121 (d) 20-96

(e) 18-63 (f) 19-71

Fig. 21 Diffusion flame structure in diverging combustor at x = 0.2 m for flight condition

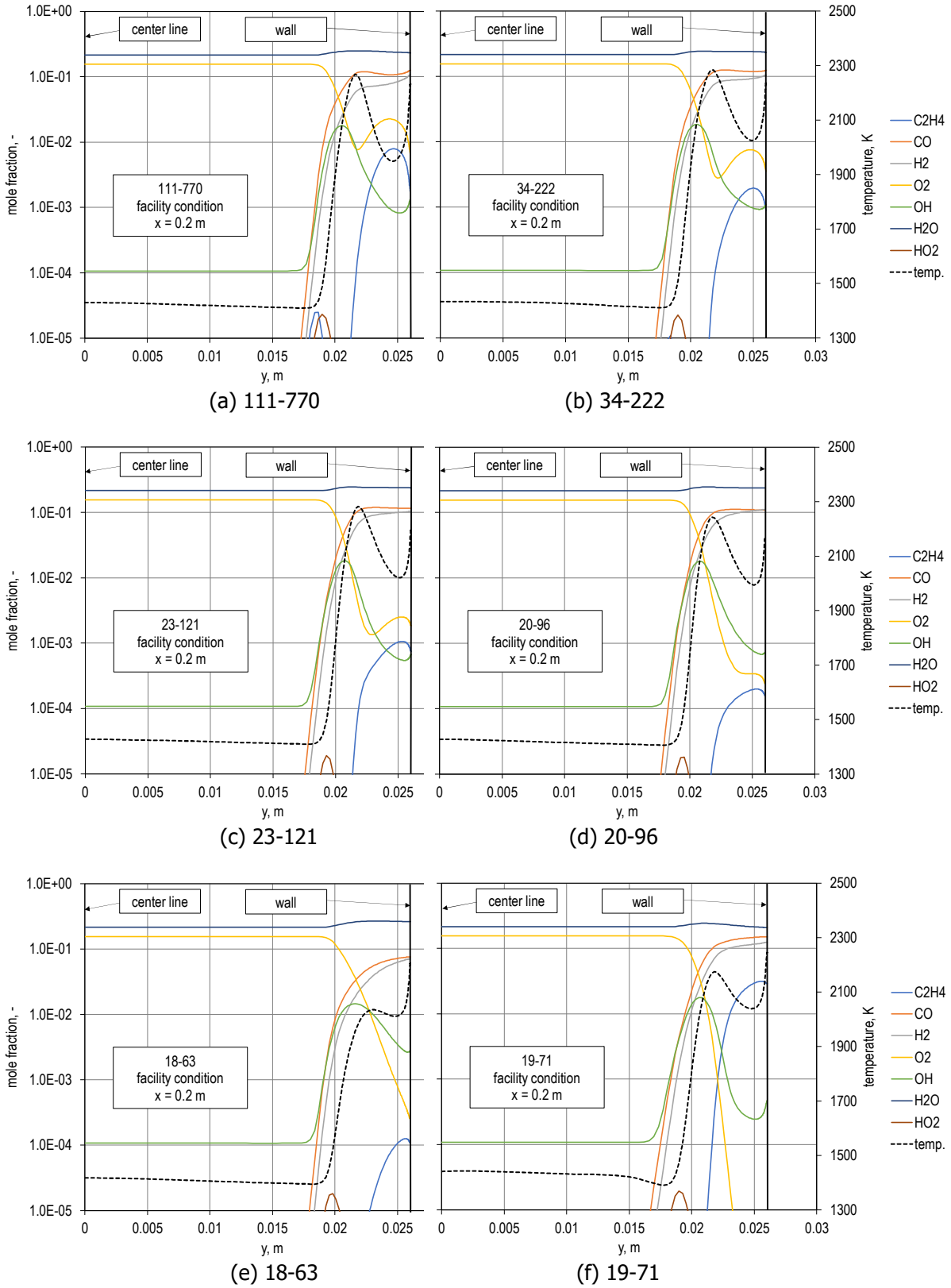

(a) 111-770 (b) 34-222

(c) 23-121 (d) 20-96

(e) 18-63 (f) 19-71

Fig. 22 Diffusion flame structure in diverging combustor at x = 0.2 m for facility condition

As another point of view, to compare the diffusion flame structure among these six reaction mechanisms (111, 34, 23, 20, 18, and 19 species mechanisms), the static temperature and mole fraction profiles in Y direction are shown in Fig. 21 (flight condition) and Fig. 22 (facility condition). All figures show the profiles at x = 0.2 m. The center line of the flow path is at y = 0 m and the solid line at y = 0.026 m shows the wall in the figure. As shown in the Figs. 15 and 16, the diffusion flame (the reaction zone) appears at the vicinity of the wall. For each condition, 34, 23, and 20 species mechanisms show similar profiles to 111 species mechanism. 18 and 19 species mechanisms show a different trend from other four mechanisms. Particularly, the peak static temperature within the reaction zone is clearly lower than that for other four mechanisms. This feature corresponds to results of 1D and 2D simulations shown above. Reaction is so sensitive to temperature that temperature profile should be precisely reproduced. Thus, 18 and 19 species mechanisms should not be selected as the reduced mechanism.

6. Validation 3: 3D reacting flow simulation

As the final validation step, 3D RANS simulation was performed to the supersonic combustor flow by using a JAXA in-house solver LS-FLOW. The LS-FLOW has been originally developed for aerodynamic simulations of an external flow around flying vehicles [7]. The solver used here is an extended version of the LS-FLOW, which can accommodate arbitrary chemical species and chemistry mechanisms. Because the 111 species mechanism cannot be applied to the 3D reacting flow simulation due to the mechanism size, the 34 species mechanism, which was evaluated as "excellent" in 0D, 1D, and 2D analyses, was applied as the master mechanism (the target of reproduction). Therefore, the 34, 23, 20, 18, and 19 species mechanisms were applied in this section. The 3D simulation was conducted by using the JAXA Supercomputer System 2 (JSS2).

Since 3D simulation requires long computational time, the computational domain was limited to be the isolator and combustor. The upstream boundary was set at 0.02 m downstream from the isolator entrance and the cross-sectional distributions of the major variables obtained from other 3D simulation for the upstream flows were given as the inflow condition. The inflow condition of the flight condition was obtained by a non-reacting 3D simulation around the forebody of the flight test model, which included the inlet and the internal flow path of the isolator. The representative flight test conditions were the flight Mach number of 6.1 and the dynamic pressure of 62.5 kPa. In the ground test case, a so-called direct-connect setup, which has been the most often used setup for the fundamental research of the combustors, was targeted in the present study. For this setup, the flow conditions of the airflow after the inlet compression are simulated by a nozzle flow of a vitiation air heater supersonic wind tunnel. The isolator is connected directly to the facility nozzle exit and the whole nozzle flow is captured into the isolator flow path. The inflow conditions for the combustor simulation were computed by another simulation of a reacting flow in the vitiation air heater facility nozzle and the isolator of the flight test model. Here, the freestream Mach number, static temperature, and static pressure of the facility nozzle flow were set to be the same as those after inlet compression in case of the flight condition. Note that, according to the vitiation air heater nozzle flow simulation, the facility flow would contain water vaper of 15% by mass and small amount of radical species. Figure 23 shows the combustor configuration for 3D simulation. Fuel is C2H4 and the equivalence ratio for the first and second stage injections are both 0.25 (0.5 in total). The detail of the combustor configuration is given in Ref. [8].

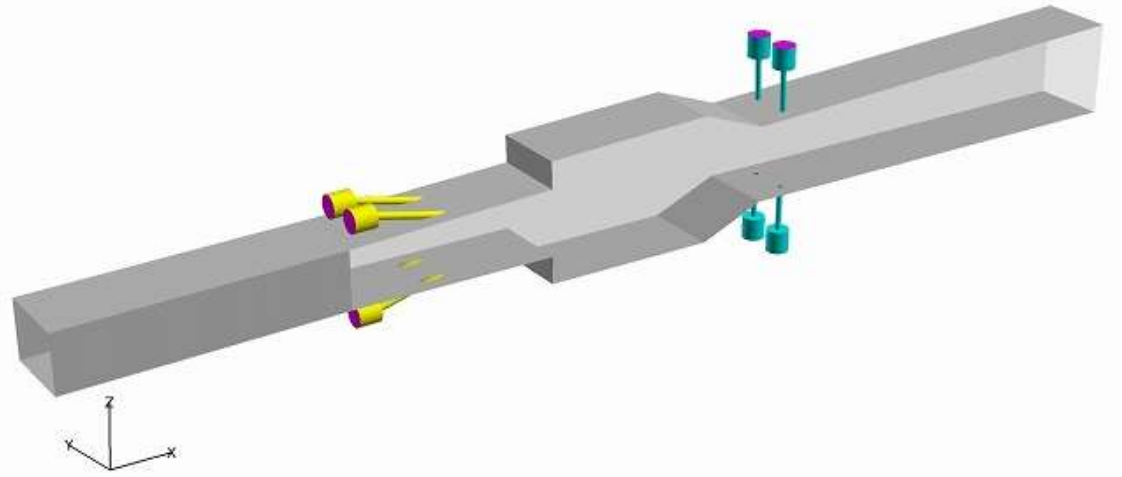

Fig. 23 Combustor configuration for 3D CFD

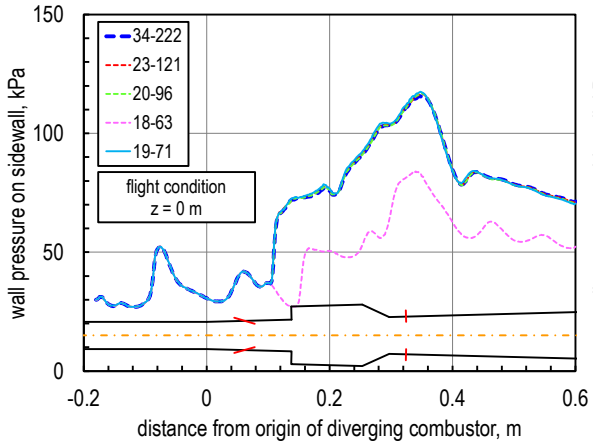

Fig. 24 Sidewall pressure (flight condition)

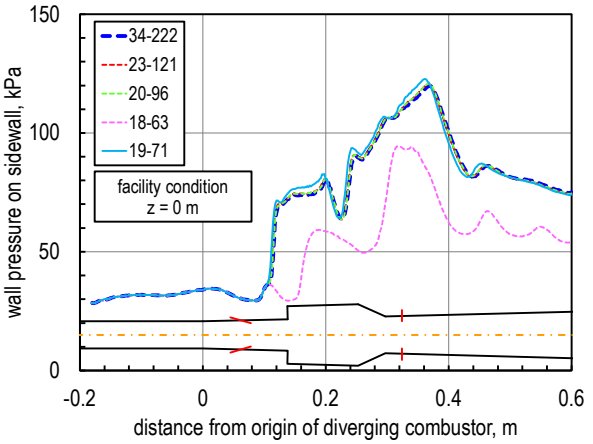

Fig. 25 Sidewall pressure (facility condition)

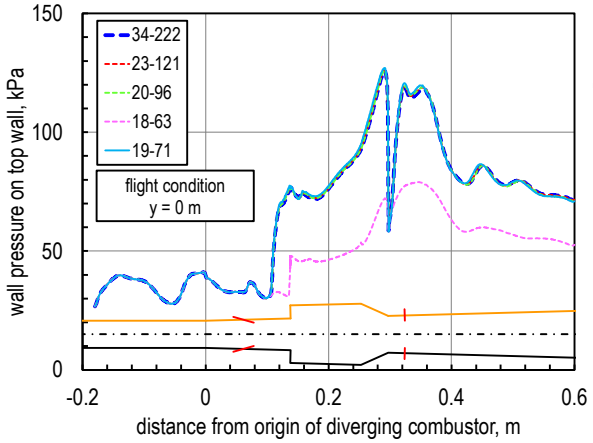

Fig. 26 Top wall pressure (flight condition)

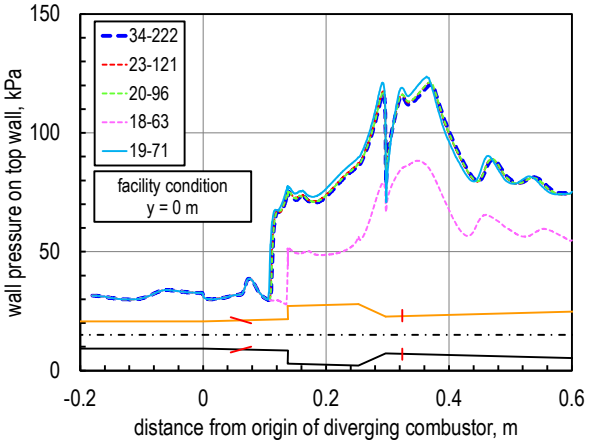

Fig. 27 Top wall pressure (facility condition)

The static pressure distributions on the sidewall are shown in Fig. 24 (flight condition) and Fig. 25 (facility condition). In addition, the static pressure distributions on the top wall are shown in Fig. 26 (flight condition) and Fig. 27 (facility condition). The 23 and 20 species mechanisms show the excellent reproducibility with the target mechanism of 34 species. As shown in the 0D, 1D, 2D, and 3D simulations, the higher the dimension, the smaller the difference in results among reaction mechanisms. This seems to be because the higher the dimension, the more complicated the reaction regions are distributed in the flow field. The 18 species mechanism shows clearly lower static pressure and temperature at downstream of the first-stage injector. The difference in reaction mechanism between 20 and 18 species mechanisms are CH2 and CH2O as shown in Table 2. Therefore, there must be the key reaction(s) in the elementary reactions including CH2 and CH2O. It should be noted that the 19 species mechanism, which was evaluated as "poor" in 0D, 1D, and 2D analyses, shows the excellent reproducibility with the target mechanism of 34 species, surprisingly. According to Table 2, the 19 species mechanism has CH2 and does not have CH2O. Thus, some elementary reactions including CH2 may be the key reactions. Sensitivity analysis will be required to find the key reactions which dominate the reproducibility.

To close the report, let us focus on the most important point of view, namely, flight condition vs. facility condition in 3D simulations. The objective of this project is to investigate the difference in static pressure distributions in the combustor between flight and facility conditions, and the objective of this report is to obtain the appropriate reduced reaction mechanism to reproduce these two kinds of static pressure distributions in 3D simulations. Figures 28-31 show the comparisons between flight (solid line) and facility (broken line) conditions for static pressure distributions on the sidewall and top wall. Each figure shows the results of 34-222 as the master mechanism and 20-96 or 19-71 as the candidate of reduced mechanism. The pressure profiles with 20-96 show the excellent agreement with those with 34-222 under both flight and facility conditions. Therefore, 20-96 can reproduce the difference between flight and facility conditions. The pressure profiles with 19-71, on the other hand, show the excellent agreement with those with 34-222 under only flight condition. As shown in Figs. 29 and 31, the error

in pressure profile under facility condition is comparable with the difference in pressure profile between flight and facility conditions. In addition, 19-71 shows clearly different features from other excellent mechanisms in 0D, 1D, and 2D analysis. So, 19-71 can have more risks to obtain the wrong conclusion than 20-96 can have. Therefore, the 20 species (96 reactions) mechanism is recommended as a reduced reaction mechanism for C2H4 fueled 3D analysis in this report. The 20 species mechanism consists of H2, O2, N2, H2O, CO2, CO, H, O, OH, HO2, CH2, CH2*, CH3, HCO, CH2O, CH3O, C2H2, C2H3, C2H4, and CH2CHO as shown in Table 2.

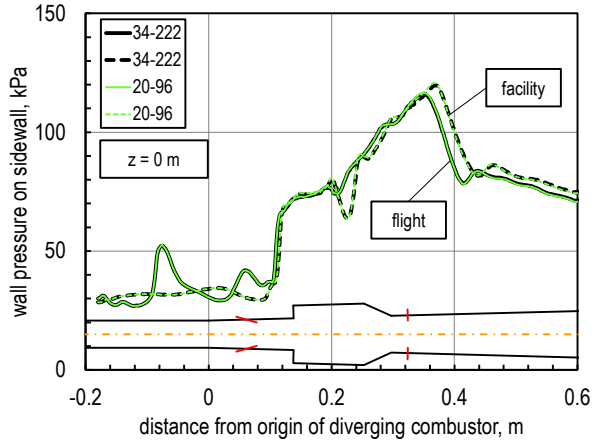

Fig. 28 34-222 vs. 20-96 (sidewall pressure)

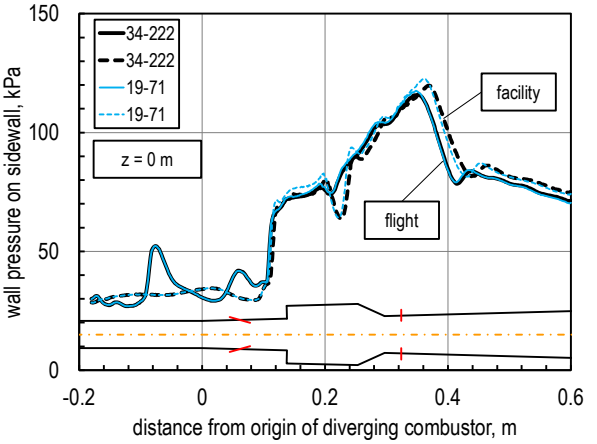

Fig. 29 34-222 vs. 19-71 (sidewall pressure)

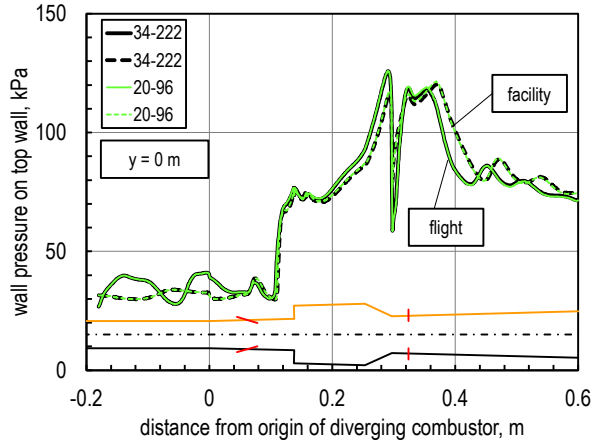

Fig. 30 34-222 vs. 20-96 (top wall pressure)

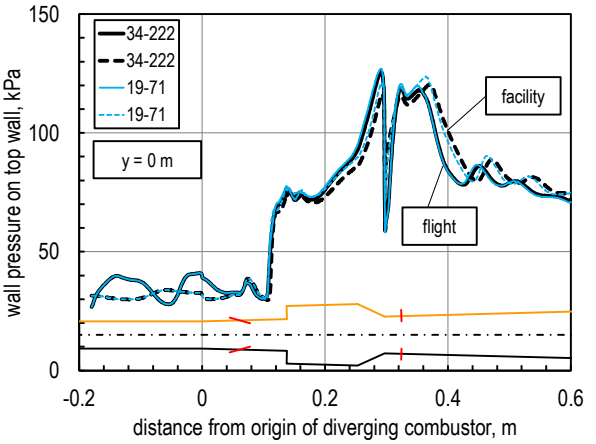

Fig. 31 34-222 vs. 19-71 (top wall pressure)

7. Conclusion

To derive a custom-made reduced reaction mechanism suitable for C2H4 fueled 3D simulation, CHEMKIN-Pro was applied. Reduction of the detailed reaction mechanism (USC Mech II) with 111 species was attempted to reproduce the static pressure distribution in the diverging combustor of the flight test vehicle. As candidates of reduced mechanism for C2H4/Air reaction, 34, 23, 20, 18, and 19 species mechanism were compared with a master mechanism, namely, 111 species mechanism. From the results of 0D ignition delay simulation and 1D, 2D, and 3D reacting flow simulations, the 20 species (96 reactions) mechanism was selected as the best reduced reaction mechanism for C2H4 fueled 3D simulation. The 20 species mechanism consists of H2, O2, N2, H2O, CO2, CO, H, O, OH, HO2, CH2, CH2*, CH3, HCO, CH2O, CH3O, C2H2, C2H3, C2H4, and CH2CHO.

Acknowledgments

The authors would like to acknowledge the contributions of T. Shimizu (Japan Aerospace Exploration Agency), J. Aono (Research Center of Computational Mechanics, Inc.), and T. Munakata (Hitachi Solutions East Japan) for their great support of this work. This work was supported by Innovative Science and Technology Initiative for Security, ATLA, Japan.

References

1. CHEMKIN-Pro version 19.2, ANSYS (2019).
2. Wang, H., et al.: USC Mech Version II. High-Temperature Combustion Reaction Model of H2/CO/C1-C4 Compounds. http://ignis.usc.edu/USC_Mech_II.htm (2007).
3. Ogawa, S., et al.: Influence on Ignition Characteristic by the Difference of Methane/Ethylene Mixture Gas Rate, 54th AIAA/SAE/ASEE Joint Propulsion Conference, AIAA 2018-4777 (2018).
4. Pepiot-Desjardins, P., et al.: An Efficient Error-Propagation-Based Reduction Method for Large Chemical Kinetic Mechanisms. Combustion and Flame. 154, 67–81 (2008).
5. Liang, L., et al.: A Dynamic Adaptive Chemistry Scheme for Reactive Flow Computations. Proceedings of the Combustion Institute. 32, 527–534 (2009).
6. CRUNCH CFD version 3.3.0, CRAFT Tech, 2019.
7. Kitamura, K., et al.: Validation of Arbitrary Unstructured CFD Code of Aerodynamic Analysis, Trans. Japan Soc. Aeronaut. Space Sci. 182, 311-319 (2011).
8. Takahashi, M., et al.: Numerical Study on Combustor Flow-Path Design for a Scramjet Flight Experiment, 32nd International Symposium on Space Technology and Science, ISTS a-32 (2019).